Simulation Study of DRMI Lock Acquisition

Qing (Rebecca) Li
Mentor: Kiwamu Izumi September 25, 2015

September 25, 2015

Abstract

Lock acquisition is the process of bringing each optic in the interferometer to its operating point. In advanced LIGO, the implementation of the Dual-Recycled Michelson Interferometer (DRMI) adds difficulties to lock acquisition due to the fact that individual cavity length signals in DRMI are highly non-linear and cross-coupled. In addition, several parameters like the choice of triggering signals, triggering threshold values, and filter shapes that have significant impacts on DRMI lock acquisition have been determined empirically and not well understood. In this project, we develop a numerical simulation of advanced LIGO using the End-To-End time domain module under realistic constrains while acquiring the flexibility of modifying the control system to study the locking behavior under different conditions.Using the simulation, we investigate the influence of possible parameters and search for the optimum method of DRMI lock acquisition.

Contents

1 BACKGROUND

1.1 Motivation

Lock acquisition is the process which brings an interferometer from its initial uncontrolled state where the suspended mirrors are swinging arbitrarily, to the final operating state where all the optical degrees of freedom are at the operating point, by controlling the distance between the mirrors [1]. The time lock acquisition takes largely determines the efficiency of observing gravitational waves. We desire the locking process to be fast, consistent and predicable, which is also the general goal of this project.

The advanced LIGO, which is the type of interferometer we work with, consists of a Dual-Recycled Michelson Interferometer(DRMI) and two Fabry-Perot (FP) arm cavities (see figure 1). DRMI is a Michelson interferometer together with the power recycling and signal recycling cavities. These two recycling cavities have increased the sensitivity as well as the locking difficulties of advanced LIGO. Currently, we are able to achieve a steady lock acquisition for the two FP cavities within about 7 minutes. However, the time it takes to lock DRMI is highly unpredictable – it varies between 2 minutes to up to 20 minutes. [2] Since the three degrees of freedom in DRMI are highly coupled, the factors causing such a difference can be rather difficult to find and understood. Therefore, the motivation of this project is to systematically study DRMI lock acquisition, investigate in different locking design, and potentially optimize DRMI lock acquisition.

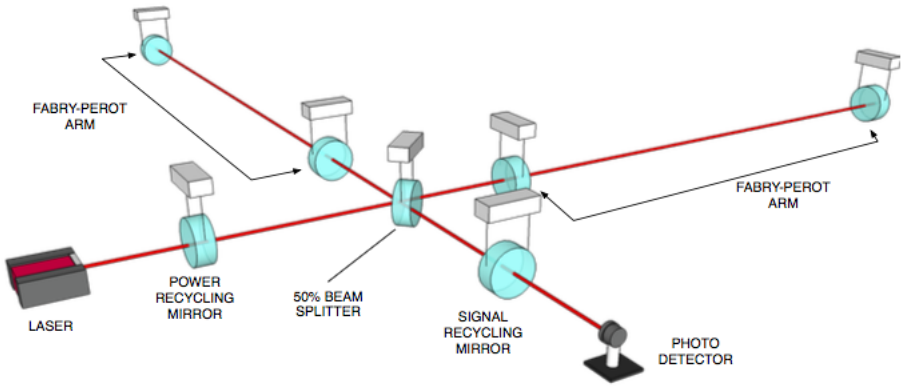

Figure 1: Diagram of a simplified advance LIGO

1.2 Definitions

The definitions of the three degrees of freedom (DOF) in DRMI, as well as the 2 DOFs for arm cavities, are specified in the diagram below.

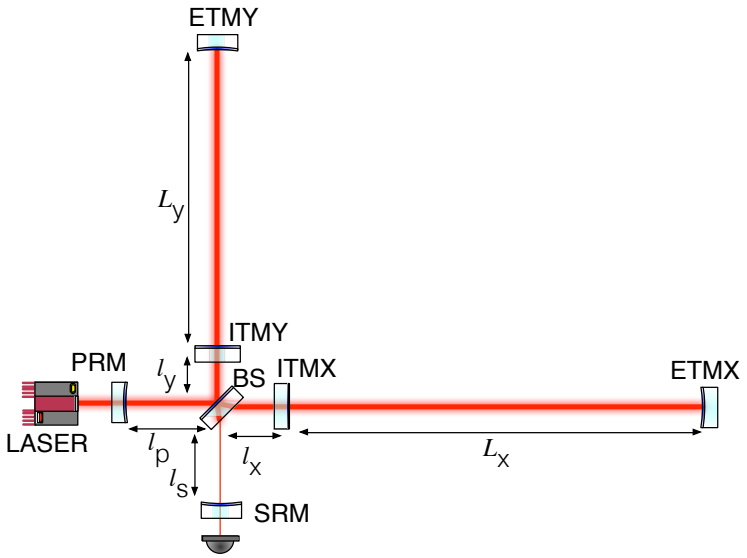

Figure 2: Definitions of degrees of freedom in aLIGO

DRMI:

$PRCL = l_p + (l_x + l_y)/2$	$PRCL$ = Power Recycling Cavity Length
$SRCL = l_s + (l_x + l_y)/2$	$SRCL$ = Signal Recycling Cavity Length
$MICH = l_y - l_x$	$MICH$ = Michelson

Arm Cavities:

$CARM = (L_x + L_y)/2$	$CARM$ = Common Arm Cavity Length
$DARM = L_y - L_x$	$DARM$ = Differential Arm Cavity Length

2 METHODS

2.1 Simulation

In this study, the End2End time domain simulation kit [3][1] was used to simulate the locking process of advanced LIGO, especially that of the Dual-Recycled Michelson Interferometer.

Previously a simulation was developed by my mentor Kiwamu Izumi in order to study other aspects of the advance LIGO lock acquisition [4], e.g. the arm length stabilization system. So in this project, I first modified the simulation[2]. so that it is more realistic with respect to DRMI lock acquisition.

[1] For more details about E2E, see http://labcit.ligo.caltech.edu/ e2e/

[2] The latest version of this simulation can be found on aLIGO dcc page at G1501041-v1

2.1.1 Setups

In the simulation, we provided a relatively ideal "outside" environment, that is, no arm cavities disturbance, for DRMI locking process so that we can focus on DRMI, while random initial positions and seismic noises were simulated to be close to reality. Since the arm cavities lock acquisition is outsides of the scope of my project, the related control system is removed from the simulation in order to save computational power.

Besides, here are a few important features in the simulation worth pointing out. In the simulation,
1. arm cavities are fully locked and CARM set out of resonance by 14 nm.
2. transfer functions for coil drivers and pendulums are taken from aLIGO documentations of realistic measurements. [5]
3. 1F PDH demodulation signals [6] are used as error signals.
4. 2F PDH demodulation signals are used as trigger signals.
5. PRM and SRM are modeled as HSTS
6. BS is modeled as BSFM

2.1.2 Control Filters

To begin with, we used the simplest control filters that work for each degree of freedom. We did not have time to explore more sophisticated control loops. Control filter shapes can be considered in future study. Details about the control filters we used in the simulation are listed in the table below.

Filter Name	Zeros	Poles	DC Gain
MICH servo filter	5,5,5	500,500,500	1.9070e+04
PRCL servo filter	100,500	10	1.1471e-04
SRCL servo filter	100,500	10	0.0076
Boost filter (for all)	3	0.3	30
BSM2 lock filter			
HSTS M3 lock filter			
HSTS M2 lock filter	1,1	0.1,20	35
HSTS M2 Elliptic filter	Order = 4	C_F = 70 Hz	R_p = 1 dB; R_s = 60 dB; G = 1.122 dB

Table 1: Table1: filter specifications

2.2 Data Collecting

Statistical data was collected using a computer cluster, Canaan, in my home institution, Gordon College physics department, in order to evaluate the performance of different locking methods with reliable amount of tests (50-100 instances). Each instance of the simulation ran independently from others and was given different random initial condition.

3 RESULTS

3.1 1F and 2F PDH Signals Study

Taking the advantage of simulation, I first measured the 1F signals and 2F PDH signals for each degree of freedom across several free spectrum ranges. In the current locking technique aLIGO utilizes, 1F PDH signals serve as error signals that indicate which side and how far the cavity is away from the desired position; while 2F PDH signals, with a simpler shape, serve as triggering signals to indicate whether the cavity is in its linear region. Below is an example of 1F and 2F signals for MICH. The complete graphs for all three degrees of freedom can be found in appendix A.

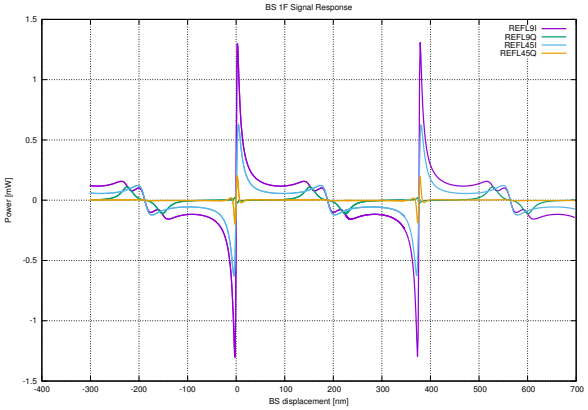

Figure 3: MICH 1F signals

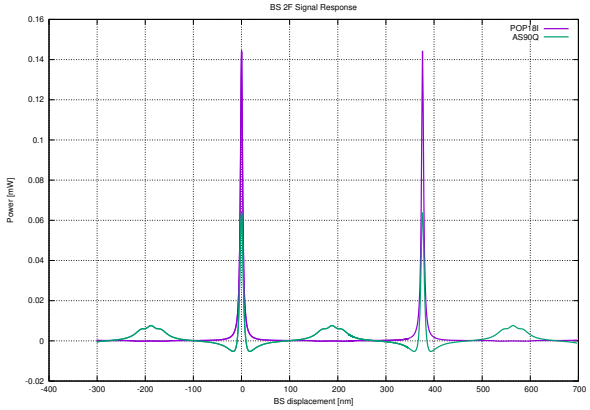

Figure 4: MICH 2F singals

3.2 Coupling Study in Linear Regions

Then I measured the 1F signals for each degree of freedom in their linear regions to obtain the displacement-to-signal coefficients. When graphing these measured values on a radar polar plot, we can clearly see that most of the signals contain displacement information for more than one degree of freedom. In order to read the correct displacements information, I adjusted the demodulation phases (equivalent as rotating the Q-I basis vectors) for each modulation frequencies (9 MHz and 45 MHz) such that an easy and clean signal decoupling method can later be applied. (e.g. REFL 45 MHz demodulation phase was adjusted so that REFL 45 Q phase contains only information of MICH displacement)

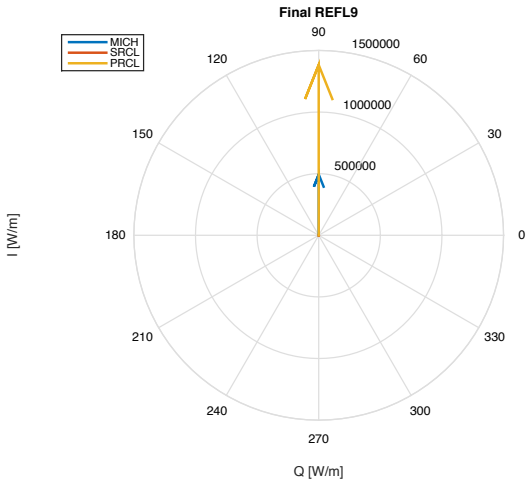

Figure 5: REFL 9 MHz

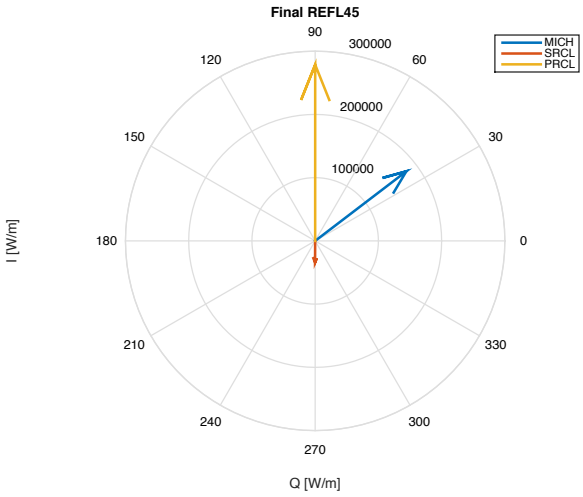

Figure 6: REFL 45 MHz Demodulation Sensing Matrix

In terms of sensing matrix, introducing demodulation phases to “clean up” error signals is equivalent as reducing the off-diagonal elements. As shown in the equation below, when the demodulation phases are adjusted, several elements become negligible compared with others in the same row. After removing

the relatively small elements and rearranging the matrix, the final form of sensing matrix is represented in the second equation.

$$\begin{bmatrix} MICH \\ SRCL \\ PRCL \end{bmatrix} = 10^{-5}[\text{m/Volts}] \begin{bmatrix} 0.003 & -0.001 & 0.513 & 0.008 \\ 0.002 & 0.251 & 0.150 & -2.081 \\ -0.001 & 0.035 & -0.184 & -0.003 \end{bmatrix} \begin{bmatrix} REFL9Q \\ REFL9I \\ REFL45Q \\ REFL45I \end{bmatrix} \quad (1)$$

$$\begin{bmatrix} MICH \\ SRCL \\ PRCL \end{bmatrix} = 10^{-5}[\text{m/Volts}] \begin{bmatrix} 0.513 & 0 & 0 \\ 0.150 & -2.081 & 0.251 \\ -0.184 & 0 & 0.035 \end{bmatrix} \begin{bmatrix} REFL45Q \\ REFL45I \\ REFL9I \end{bmatrix} \quad (2)$$

So in our simulation, MICH uses REFL45 Q phase as error signal; SRCL mainly uses REFL45 I phase, but also REFL45 Q phase and REFL 9 I phase to decouple MICH and PRCL; PRCL uses mainly REFL9 I phase, but also REFL 45 Q phase to decouple MICH.

3.3 Coupling Study Outside Linear Regions

It is not too complicated to decouple error signal of one degree of freedom from another's if both of them are in their linear regions, as shown above. However, decoupling can be impossible when the linear relation no longer holds. Also, since all three degrees of freedom in DRMI are coupled in error signals, it is extremely difficult to understand how they influence each other if we try to study all three at the same time. Therefore I broke the three degrees of freedom into three pairs and studied each pair independently from the third one.

To explain what was done exactly, I will take the SRCL-PRCL pair as an example. In the simulation, I disabled all interference from MICH, namely turning off all the noise on MICH and its control feedback, as if MICH is locked perfectly. When studying the impact on SRCL's signal response from PRCL displacement, I would lock PRCL at certain distance from its resonance point and scan the signal response for SRCL. Since it would be too much work, also unnecessary, to collect data for PRCL at each possible location, I selectively set PRCL to be around the mid point between two resonance points, because it is where normally signals switch signs. Sign switching is what would cause locking failures (imagining what happens when pushing the mirrors towards the opposite direction as desired) and exactly what we need to avoid.

Below are the error signal for SCRL with and without PRCL offset from resonance point by 270 nm (1/2 free spectrum range + 3nm). Note the y axis scales are different in figure 7 and figure 8. Comparing the two graphs with and without PRCL offset, we can see that the error signal is completely distorted due to the displacement in PRCL.

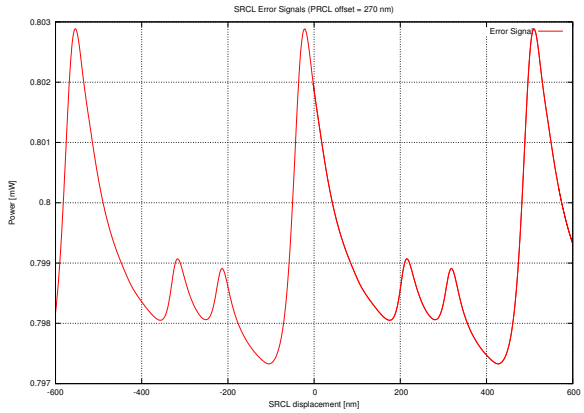

Figure 7: SRCL error signal with PRCL displacement of 270 nm

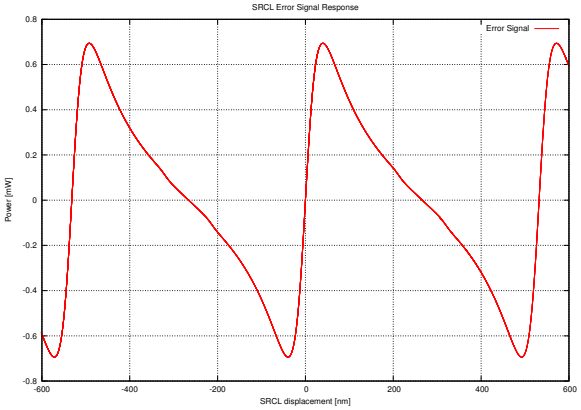

Figure 8: SRCL error signal without PRCL displacement

However, SRCL offset barely has any effect on PRCL error signal as shown in the two caparison graphs below.

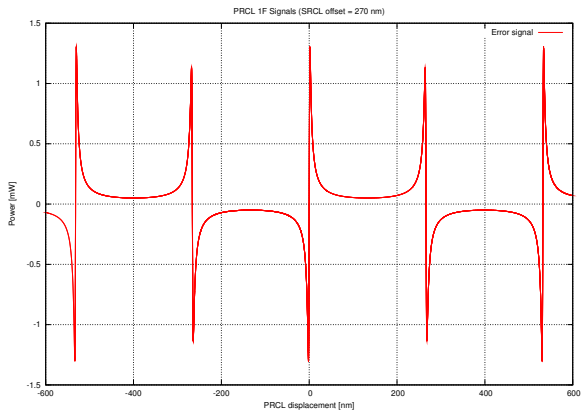

Figure 9: PRCL error signal with SRCL displacement of 270 nm

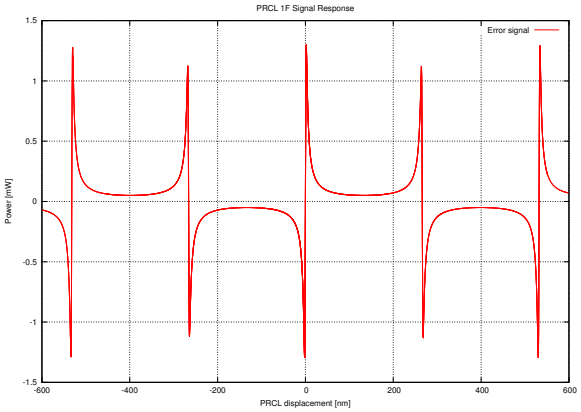

Figure 10: PRCL error signal without SRCL displacement

What we can conclude from these results is that SRCL is more sensitive to PRCL displacement and its error signal would switch signs if PRCL is not in the linear region, while PRCL has more robust error signal that SRCL has no apparent influence on.

Similar studies was completed on the other two pairs (MICH PRCL and MICH SRCL). More detailed results for all three pairs of degrees of freedoms can be found in Appendix B. The results can be described in a more general and abstract diagram below, where the color red represent that one DOF displacement would flip the error signal sign of the one being pointed at; green represents no such impact on the pointed one. The boldness of the arrow represents how strong the influence is – MICH is more susceptive to PRCL displacement and PRCL is to MCIH. This influence triangle serves as the underlying principle of designing a locking sequence that I will talk about in the next section.

Figure 11: Influence triangle of one DOF's displacement to other DOFs' error signals

3.4 Locking Sequence Study

In the simulation, there are three states in the locking process for each degree of freedom: 0 represents the waiting process when the cavity is out of the linear region and no control in engaged; 1 represents the locking process when control loop is engaged to grab the mirror that swings to the linear region and lock it at its operating point using only the bottom stage actuators (beam splitter uses the second stage since it does not have any actuators on the bottom stage); 2 represents that all three DOFs are locked, and that the actuators on the second stage and low frequency boost filters are engaged to help stabilize optics' movements due to the low frequency seismic noise.

Having understood the general influence that the three degrees of freedom have on each other, I then started designing a locking sequence that is based on the previous study. For a pair like PRCL and SRCL where one is more sensitive to the other, it is necessary that PRCL is locked before any control applied to SRCL. Otherwise, wrong error signal will be used in locking SRCL and it may cause SRCL being pushed out of its linear region and loses lock. As for other pairs where both DOFs have significant influence on each other, locking should start only when both DOFs are in linear region.

Besides the logic stated above, there are also several other aspects that we need to take into account:
1. Beam splitter only has actuators on the top two stages –we do not have control on the bottom stage. This results in a high displacement to force gain at low frequency, which makes MICH extremely responsive to any mistake in reading error signal. Therefore, MICH control should only be engaged when we are positive that all three DOFs are in linear region and are relatively stable.

2. Since PRCL has the most robust error signal, we may consider introducing some mistakes on purpose to increase the frequency that PRCL across its linear region. However, PRCL could only possibly be locked when MICH is in its linear region, since it Therefore, in this study, we engage PRCL control loop regardless of other DOF's states.

With the those rationale stated, the designed locking sequence can be represented in the block diagram below.

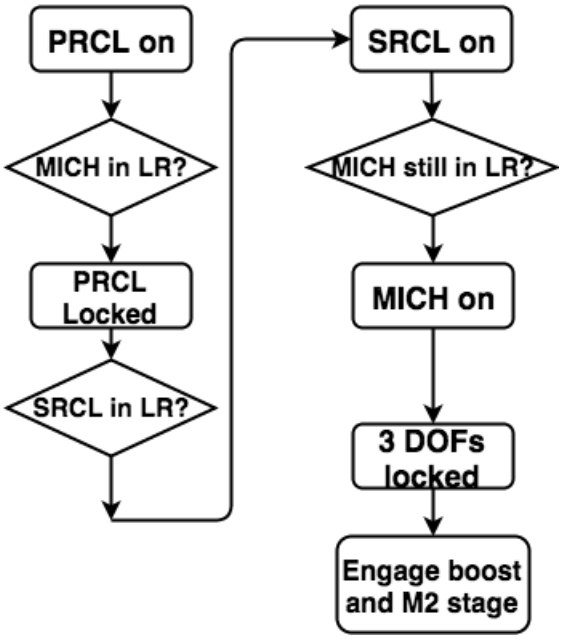

Figure 12: Locking states illustration

3.5 Double Triggers Investigation

As mentioned in the previous sections, 2F PDH demodulation signals are used as triggering signals, but I did not explain how exactly they function as triggers. Here I will explain a little more before proceeding. The general idea is to use one or more 2F signals are Schmitt triggers with a designed delay. Once the triggering signal goes above the higher threshold value, we engage the control loop, and starting counting – locking state 1. When the triggering signal has stayed above the higher threshold for a certain waiting time (set as 1 sec in the simulation), the simulation take it as the cavity is locked and then proceed to locking state 2. If the triggering signal drops below the lower threshold at any point in the process, control loop will be disengaged and the system be brought back to the waiting state 0. This process might be illustrated clearer in the graph below.

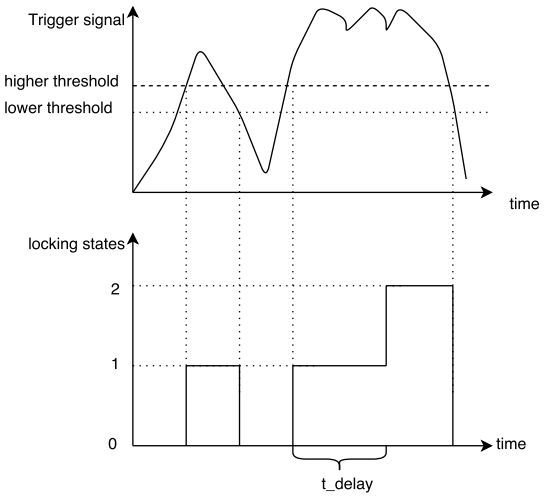

Figure 13: Demonstration of trigger functions

3.5.1 Why Double Triggers

Currently LIGO Hanford and Livingston both use POP 18 MHz as the only triggering signal for all three DOFs. POP 18 signal goes up when PRCL and However, POP18 is not sensitive to SRCL as shown in figure 14: it stays high as long as the MICH and PRCL are locked – POP18 is not a good indicator for SRCL. On the contrary, AS 90 MHz signal, plotted as the green line in the graph, is a much better indicator for SRCL. In fact, AS90 is proven to be sensitive to all three DOFs (see graphs in appendix A) – it shoots up when all three DOFs are near their resonance points.

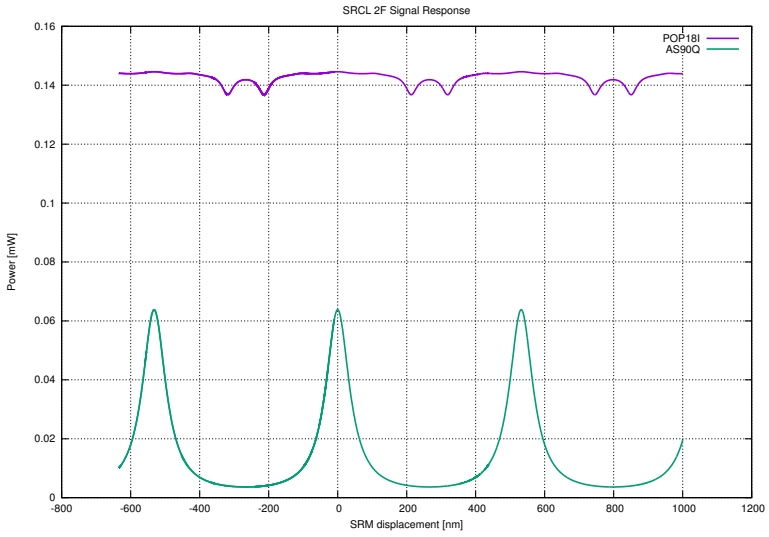

Figure 14: POP18 and AS90 signals for SRCL

However, there's is a downside of using AS90 as the only triggering signal – AS90 also goes up when the three DOFs meet some other conditions, which are not well studied. But the point is, it is

not necessary that all three DOFs are in linear regions when AS90 goes up.

To solve the dilemma here, I decided to try using both POP18 and AS90 as double triggers. Since POP18 only goes up when both MICH and PRCL are close to their resonance points, we can be positive to say that SRCL is also near its resonance point if AS90 is high at the same time.

Another reason of using double triggers lies in the susceptivity of MICH to PRCL displacements. Not only when PRCL is offset by about 1/2 free spectrum range, even a small displacement in PRCL as 20 nm could cause MICH error signal to behave in an odd way. An example is shown in figure 15 and 16, the center of MICH 1F signals are displaced when PRCL has an offset of 20 nm. AS90 displays a more obvious indication than POP18 of such situation and prevent MICH from being locked at other location than the desired point.

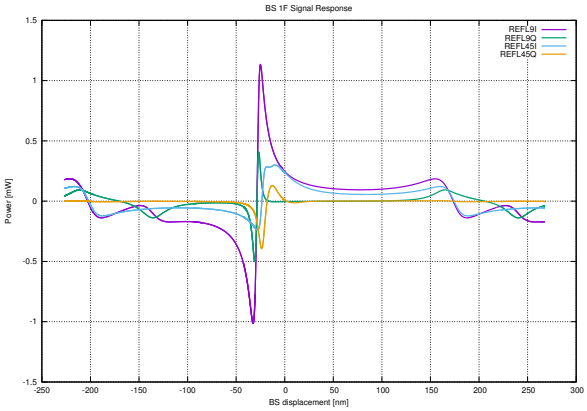

Figure 15: MICH 1F signals with PRCL offset by 20 nm

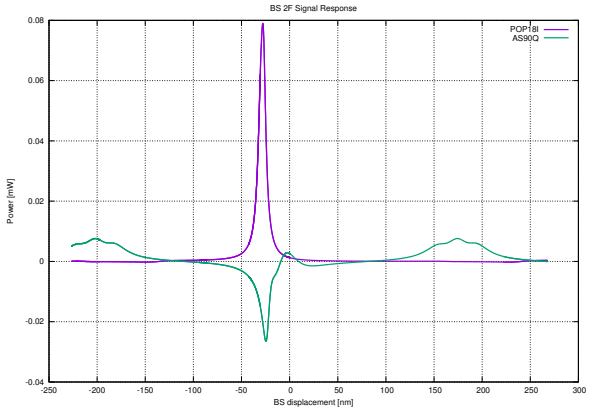

Figure 16: MICH 2F signals with PRCL offset by 20 nm

3.5.2 Double Trigger Performance

To show how double triggers work in the simulation, I will use one of the successful lock as an example. Figure 17 contains three plots of the same event: position plot of the three mirrors associated with the 3 DOFs, triggering signals plot for POP18 and AS90, and locking state plot for the 3 DOFs. In this example, DRMI is locked at around 60 sec. First, PRCL is stabilized at its 0th resonance point since MICH is also near its 1st resonance point; then SRCL gained lock soon after PRCL; finally when both PRCL and SRCL are locked, MICH control is engaged and all three DOFs are then successfully locked. After waiting for 1 sec, all three DOFs proceed into locking state 2 where the second pendulum stage and low frequency boost are engaged.

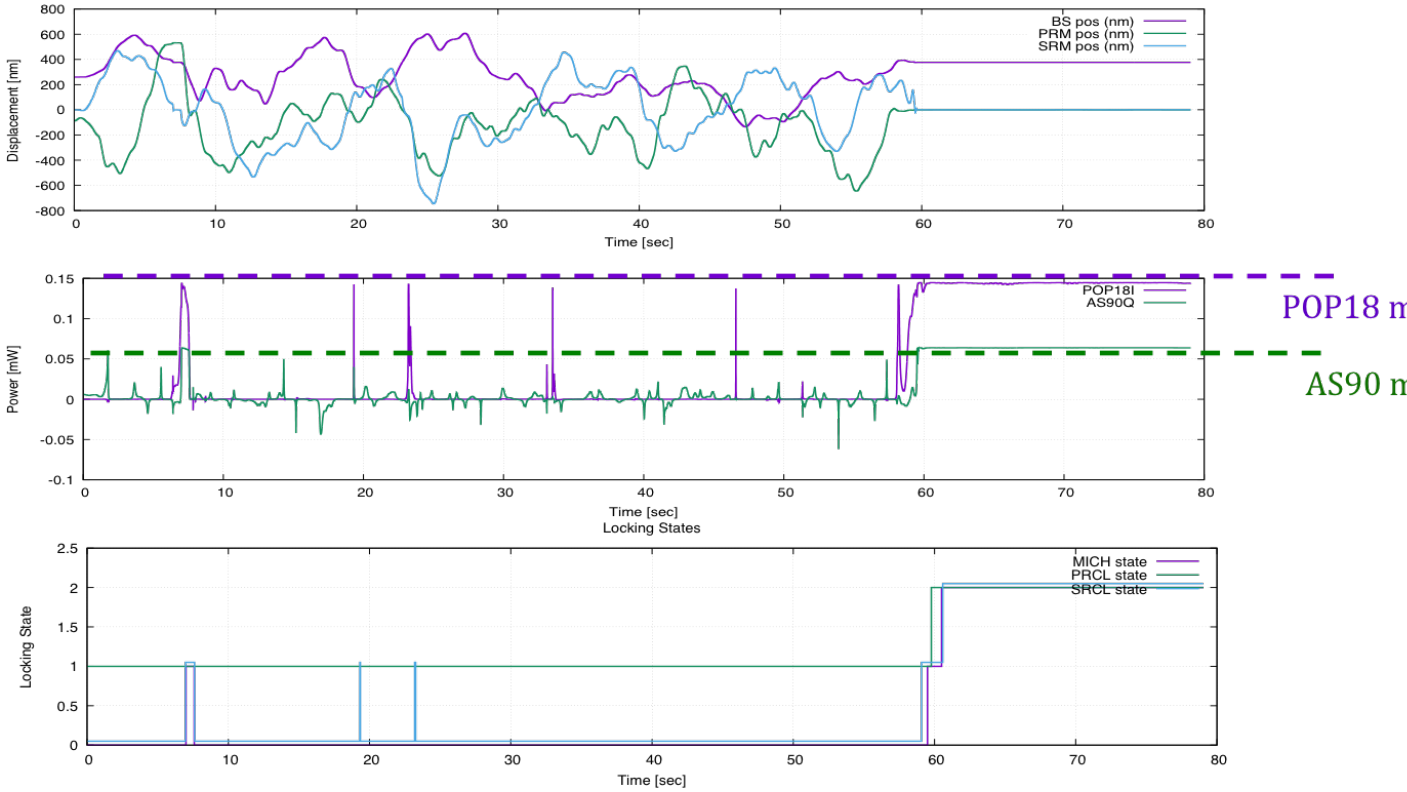

Figure 17: POP18 and AS90 signals for SRCL

After implementing the locking sequence in the simulation, I tested the performance of double triggers with decent number of tests to provide reliable results. The histogram below shows the locking time distribution from 70 attempts. For 46% of the time, DRMI was locked within 2 minutes; 75% locking attempts succeeded within 5 minutes. This data gives a mean locking time of 193 sec, and a median locking time of 147 sec.

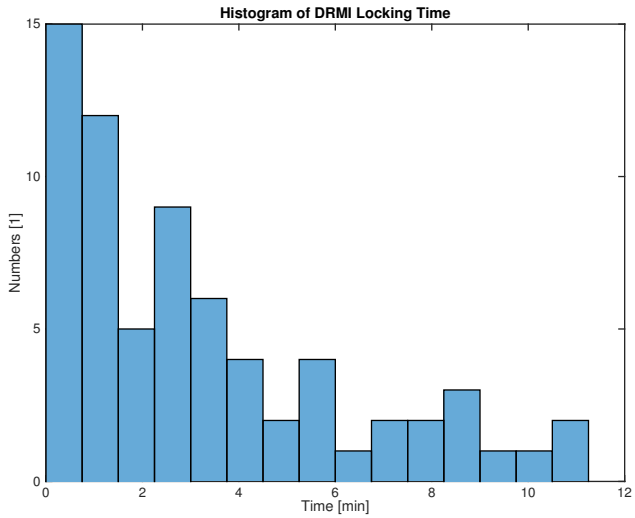

Figure 18: Locking time distribution with double triggers

In theory, the double triggers scheme should provide a more reliable performance than the single trigger scheme. However, I did not have a chance to collect statistical data for the single trigger performance due to the limited time for this project. This work should be considered in future study.

4 CONCLUSIONS and FUTURE WORK

In this project, we utilized computational simulation to study the DRMI lock acquisition and investigate in double trigger locking scheme. We acquired better understanding of the coupling relations among the three degrees of freedom in DRMI both inside and outside their linear regions. Using the understanding from the coupling study, we designed and tested the double triggers locking scheme, and obtained promising results.

Further work would include study on the control filter shapes, deeper investigation on the threshold values setting, and collecting statistical data of single trigger performance for comparison purpose.

5 Acknowledgments

This research was conducted under Caltech?s Summer Undergraduate Research Fellowship program at the LIGO Hanford Observatory and was funded by the National Science Foundation.
I would like to thank my mentor, Kiwamu Izumi, for patiently teaching me so much without complains, and guiding me through difficulties we encountered. I would also like to thank everyone else at LHO for helping make this project a successful one, and this internship a unforgettable experience.

A Measured 1F and 2F Signals without Coupling

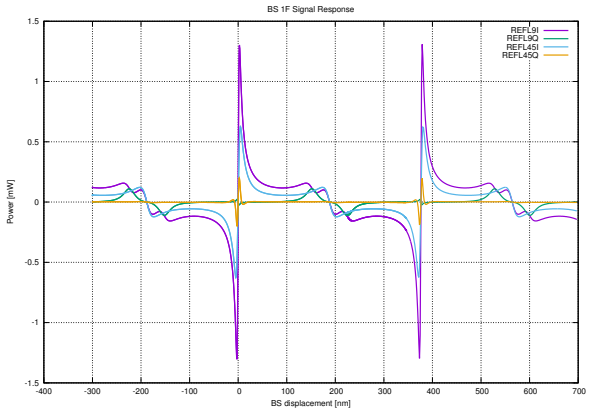

Figure 19: MICH 1F signals

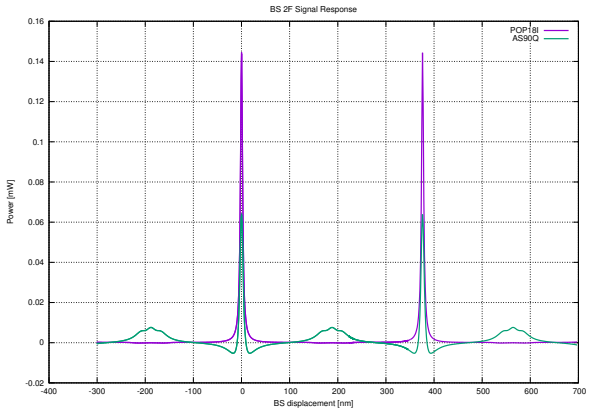

Figure 20: MICH 2F singals

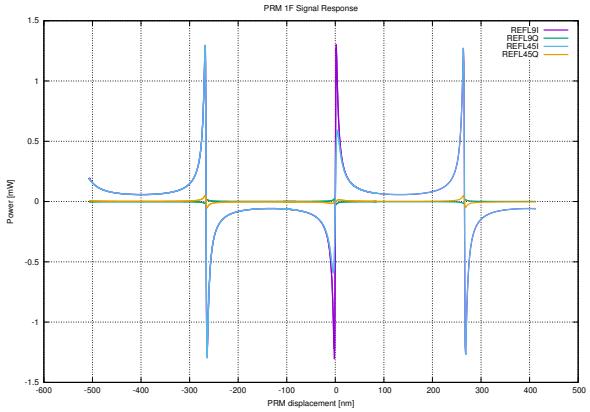

Figure 21: PRCL 1F signals

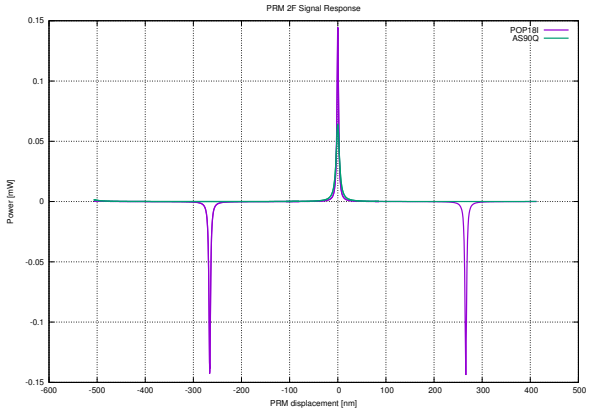

Figure 22: PRCL 2F singals

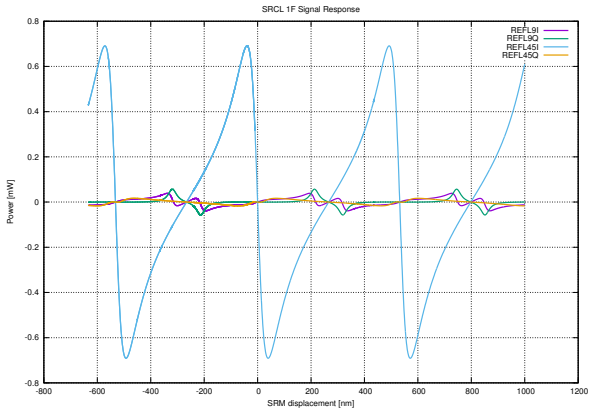

Figure 23: SRCL 1F signals

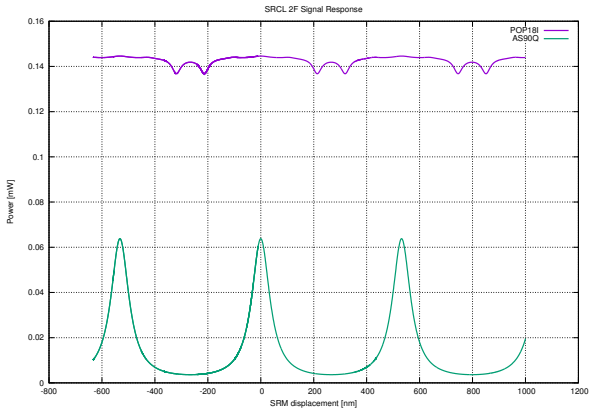

Figure 24: SRCL 2F singals

B Measured 1F and 2F Signals with coupling

B.1 MICH with PRCL offset by 270 nm

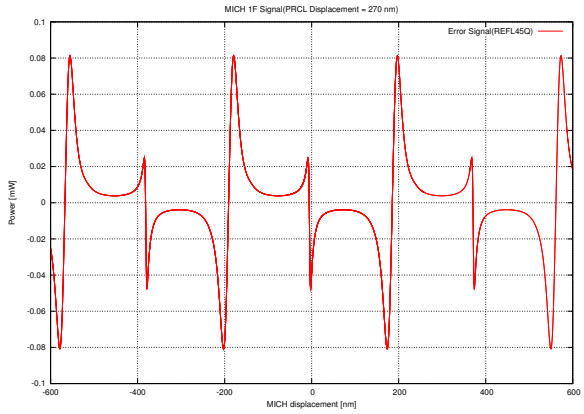

Figure 25: MICH Error Signal with PRCL offset by 270 nm

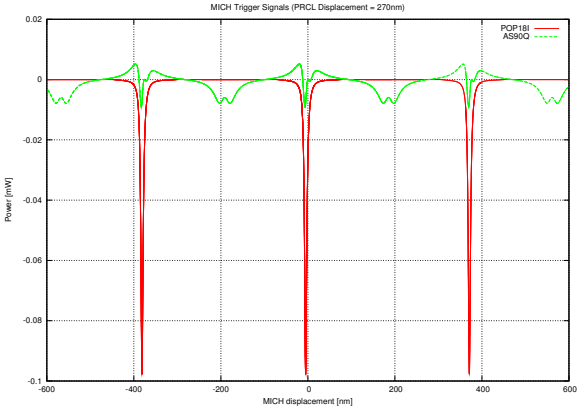

Figure 26: MICH Triggering Signals with PRCL offset by 270 nm

B.2 MICH with SRCL offset by 270 nm

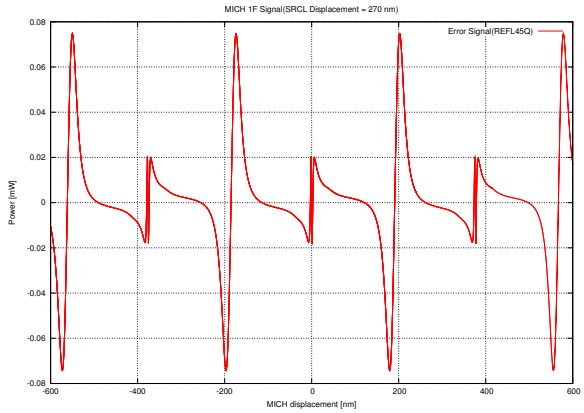

Figure 27: MICH Error Signal with SRCL offset by 270 nm

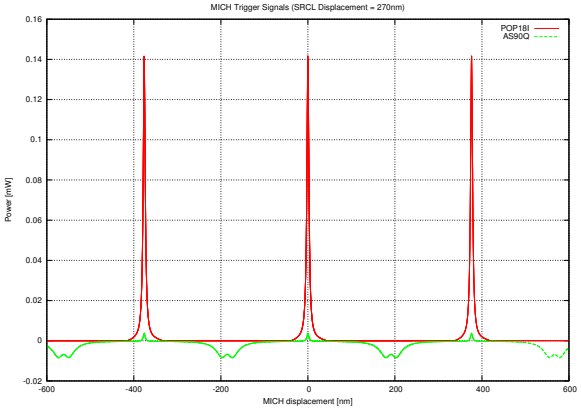

Figure 28: MICH Triggering Signals with SRCL offset by 270 nm

B.3 PRCL with MICH offset by 189 nm

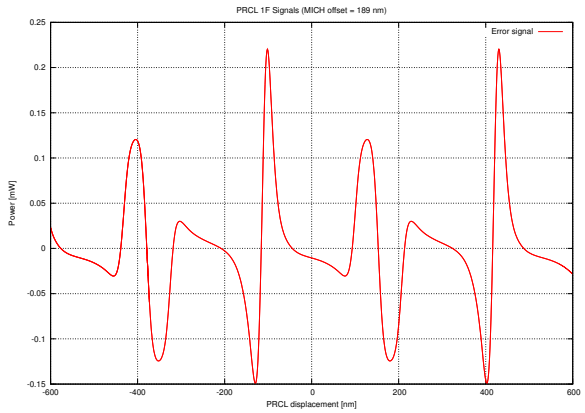

Figure 29: PRCL Error Signal with MICH offset by 189 nm

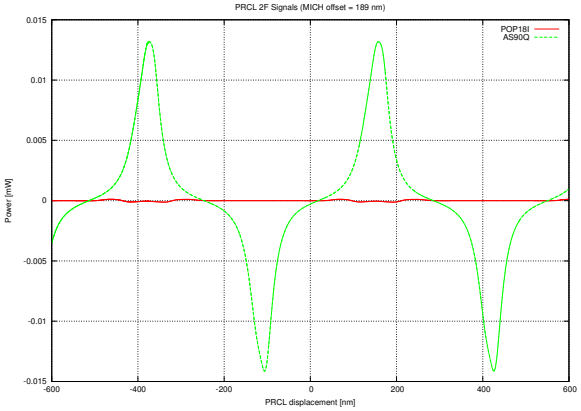

Figure 30: PRCL Triggering Signals with MICH offset by 189 nm

B.4 PRCL with SRCL offset by 270 nm

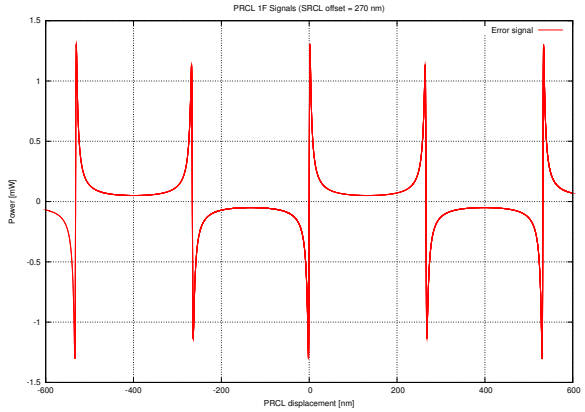

Figure 31: PRCL Error Signals with SRCL offset by 270 nm

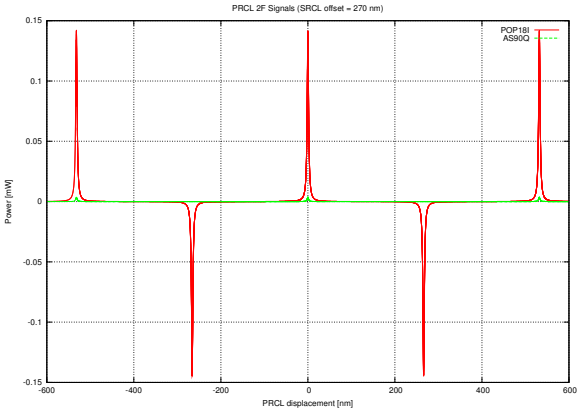

Figure 32: PRCL Triggering Signals with SRCL offset by 270 nm

B.5 SRCL with MICH offset by 189 nm

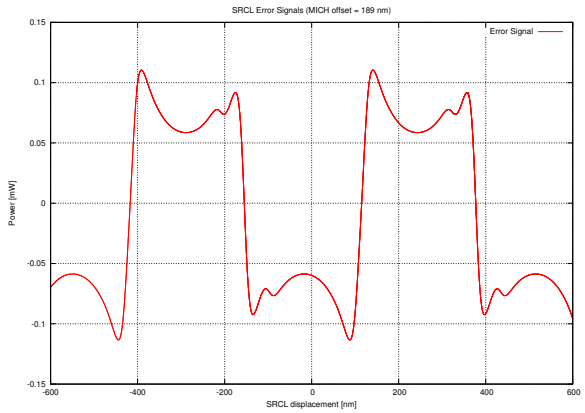

Figure 33: SRCL Error Signal with MICH offset by 189 nm

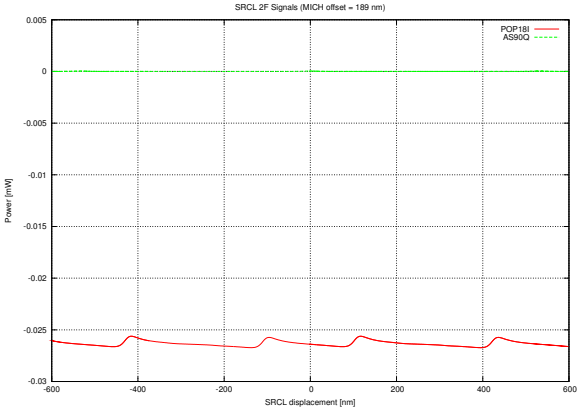

Figure 34: SRCL Triggering Signals with MICH offset by 189 nm

B.6 SRCL with PRCL offset by 270 nm

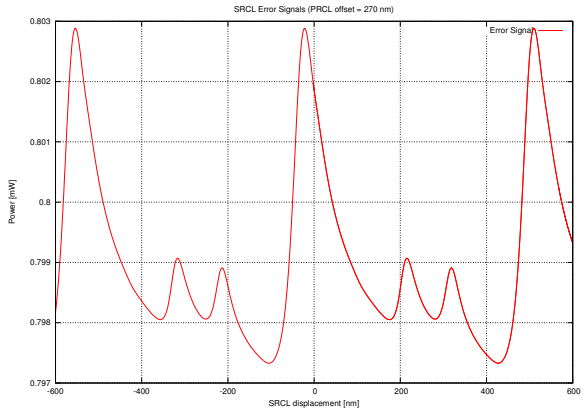

Figure 35: SRCL Error Signal with PRCL offset by 270 nm

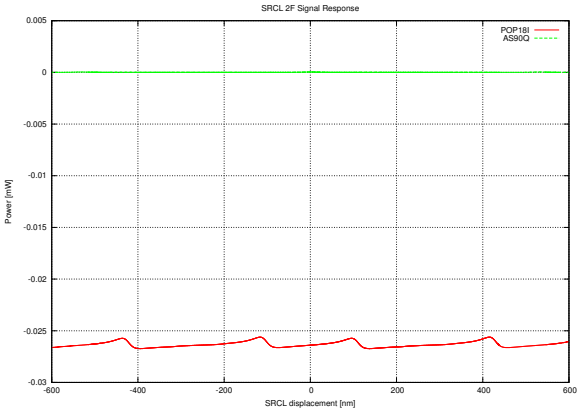

Figure 36: SRCL Triggering Signal with PRCL offset by 270 nm

References

[1] K. Izumi, *Multi-Color Interferometry for Lock Acquisition of Laser Interferometric Gravitational-wave Detectors*. PhD thesis, University of Tokyo, 2012.

[2] S. Dwyer, "A look at duty cycle for the first week of er7." https://alog.ligo-wa.caltech.edu/aLOG/index.php?callRep=19075.

[3] H. Yamamoto, M. Barton, B. Bhawal, M. Evans, and S. Yoshida, "Simulation tools for future interferometers," *Journal of Physics: Conference Series* **32**(1), p. 398, 2006.

[4] L. B. Kiwamu Izumi, Sheila Dwyer, "Simulation study for aligo lock acquisition." LIGO-T1400298–v1, 05 2014.

[5] N. A. R. J. S. Kissel, *Beam Splitter / Folding Mirror Suspension (BSFM) Actuation Ranges*. LIGO-T1100602-v2.

[6] E. D. Black, "An introduction to pound–drever–hall laser frequency stabilization," *merican Journal of Physics* **69**(1), pp. 79–87, 2001.